JACS
JOURNAL OF THE AMERICAN CHEMICAL SOCIETY
Article
pubs.acs.org/JACS

Chain Length and Solvent Control over the Electronic Properties of Alkanethiolate-Protected Gold Nanoparticles at the Molecule-to-Metal Transition

Anthony Cirri, Alexey Silakov, Lasse Jensen, and Benjamin J. Lear*

Department of Chemistry, The Pennsylvania State University, University Park, Pennsylvania 16802, United States

Supporting Information

ABSTRACT: Alkanethiolate protected gold nanoparticles are one of the most widely used systems in modern science and technology, where the emergent electronic properties of the gold core are valued for use in applications such as plasmonic solar cells, photocatalysis, and photothermal heating. Though choice in alkane chain length is not often discussed as a way in which to control the electronic properties of these nanoparticles, we show that the chain length of the alkyl tail exerts clear control over the electronic properties of the gold core, as determined by conduction electron spin resonance spectroscopy. The control exerted by chain length is reported on by changes to the g-factor of the metallic electrons, which we can relate to the average surface potential on the gold core. We propose that the surface potential is modulated by direct charge donation from the ligand to the metal, resulting from the formation of a chemical bond. Furthermore, the degree of charge transfer is controlled by differences between the dielectric constant of the medium and the ligand shell. Together, these observations are used to construct a simple electrostatic model that provides a framework for understanding how surface chemistry can be used to modulate the electronic properties of gold nanoparticles.

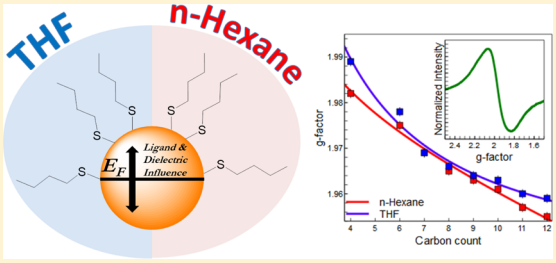

INTRODUCTION

Organic soluble, monolayer-protected metal nanoparticles have become ubiquitous in science and engineering due to their ease of synthesis, stability, and unique electronic properties; all of which make them desirable for use in applications such as molecular electronics,[1] plasmonic photocatalysts,[2] and plasmon-based chemical sensors.[3] The breadth of this utility ultimately rests upon the ability to rationally tune their electronic properties. At present, it is well established that changes in size, geometry, and dielectric environment can be used in a rational manner to tune the electronic properties of these particles, which enables applications for nanoparticles in photovoltaics, photocatalysis, and photothermal heating.[4−6] Comparatively little is known concerning how the surface chemistry of these particles can be used to control their electronic properties, despite the fact that a diverse set of chemical architectures exist that are compatible with metal particle surfaces and that both chemical intuition and the vast literature of inorganic chemistry testify to the control that covalently bound ligands exert over the electronic structure of metal centers.

Work examining the influence of surface chemistry over the electronic properties of metal nanoparticles has been largely performed on gold nanoaprticles (AuNPs), which are the prototypical metal nanoparticle. At present, it is appreciated that changes in the ligand binding group, such as amine to thiolate, is capable of imparting profound changes to the physical properties of AuNPs, including superparamagnetic behavior, dampening of the surface plasmon resonance, and increased electron−lattice coupling.[7,8] Recent work from Portehault and co-workers,[9] as well as ourselves,[10,11] demonstrates that changes to the tail group of aromatic thiolate ligands produces measurable changes in the electronic properties of the metallic core. However, with one notable exception,[12] very little is known concerning electronic properties of AuNPs and the ligands that dominate the literature of AuNPs: alkanethiols. This, in turn, means that though AuNPs are often employed for their unique electronic properties, these electronic properties are not controlled to the full extent that they could be.

To a large extent, the lack of knowledge concerning the impact of choice in alkanethiols is due to the lack of a probe sensitive enough to detect changes; with plasmonic features[13] or electrochemistry[14] unable to resolve effects of changes in the alkanethiolates. Recent work from our laboratory has shown that conduction electron spin resonance (CESR) is a tool with selectivity for electrons at the Fermi level (E_F) in metals and sufficient sensitivity to easily resolve the electronic effects of changes in aromatic thiolates.[10,11] Herein we show that CESR also has the ability to resolve the effects of changes in alkane chain length by using a series of AuNPs protected with butanethiolate (C4), hexanethiolate (C6), heptanethiolate (C7), octanethiolate (C8), nonanethiolate (C9), decanethiolate (C10), undecanethiolate (C11), or dodecanethiolate (C12). In particular, we find that these ligands exert a clear electrostatic influence over the surface potential of the particles, with the surface

Received: September 12, 2016
Published: November 8, 2016

DOI: 10.1021/jacs.6b09586
J. Am. Chem. Soc. 2016, 138, 15987−15993

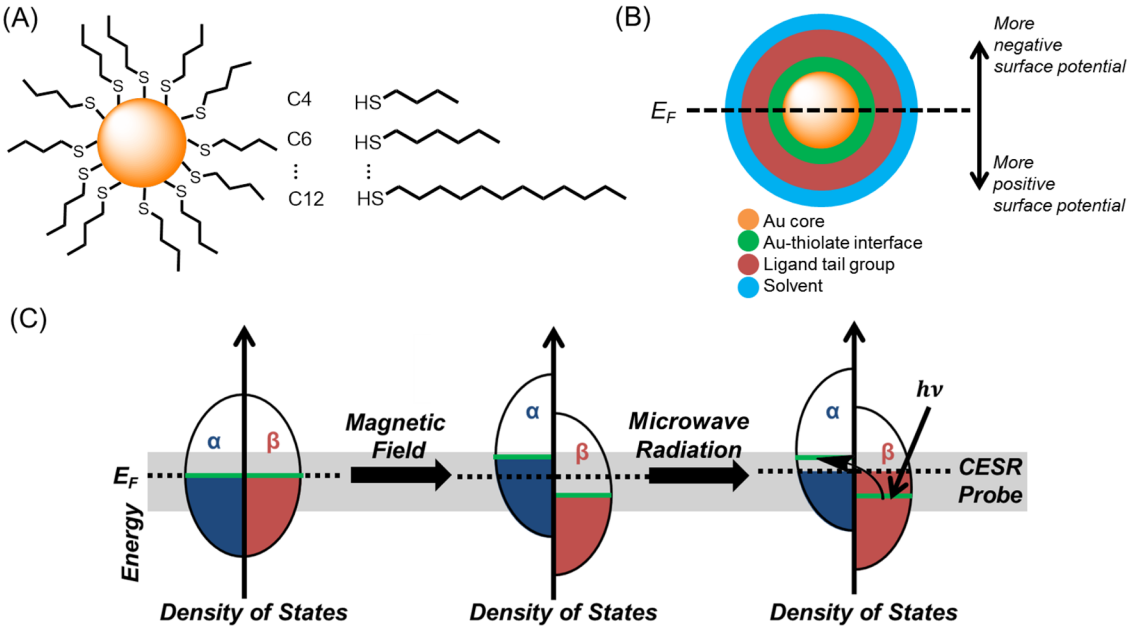

Figure 1. Schematic of the experimental approach. (A) A series of gold nanoparticles were prepared with a protecting layer of alkanethiolates (butanethiolate to dodecanethiolate) and were analyzed by conduction electron spin resonance (CESR) to observe the effect that changes to either (B) the alkyl tail group or solvent have upon the electronic properties of the metallic core near the Fermi energy (E_F). (C) Pauli paramagnetism of the gold nanoparticles gives rise to the CESR signal. In the absence of an external magnetic field, the α and β spin-states of the valence band are degenerate. Application of an external magnetic field breaks this degeneracy and leads to a number asymmetry in the α and β spin populations. Using microwave radiation, a transition between the two spin states may be achieved. The spin-flip is sensitive to, and selective for, those electrons near the E_F, and can be used to report on the electronic properties of the metallic core near the E_F.

potential increasing as a function of alkane chain length (Figure 1).

MATERIALS AND METHODS

The following chemicals were purchased from Sigma-Aldrich: butanethiol (97%), hexanethiol (95%), heptanethiol (98%), octanethiol (98.5%), nonanethiol (95%), undecanethiol (98%), dodecanethiol (98+%), sodium borohydride (98%), THF (>98%), and *n*-hexane (97%). Tetraoctylammonium bromide (>98%) and chloroauric acid trihydrate (99.999%) were purchased from Alfa Aesar, and toluene was purchased from Aqua Solutions. All chemicals were used as received without further purification.

Synthesis of AuNPs. AuNPs protected with butanethiolate (C4), hexanethiolate (C6), heptanethiolate (C7), octanethiolate (C8), nonanethiolate (C9), decanethiolate (C10), undecanethiolate (C11), and dodecanethiolate (C12) were prepared via the Brust method. The details of the general procedure may be found elsewhere;[10] however, it is important to note that for each synthesis a $HAuCl_4 \cdot 3H_2O$-to-alkanethiol ratio of 0.90:2.81 mmol was used in this study.

Characterization. CW-CESR measurements were performed using a Bruker ESP 300 X-band spectrometer with an ER 041MR microwave bridge and an ER 4116DM cavity operating in the perpendicular TE102 microwave mode (ν_{mw} = 9.623 GHz). Temperatures of 25 K were achieved using an ER 4112-HV Oxford Instruments variable temperature helium flow cryostat. The following parameters were used for collecting all spectra: microwave power, 200 mW; modulation amplitude, 2 G; time constant, 40.96 ms; conversion time, 39.06 ms; number of points, 4096. Saturated solutions of AuNP samples were prepared with *n*-hexane or THF, degassed by sparging with argon, and sealed with paraffin wax tape in clear fused quartz tubes with 4 mm O.D./3 mm I.D. Following CW-CESR analysis, the particles were sized using a JEOL2010 TEM with a LaB_6 emission source and an accelerating voltage of 200 kV. Dilute samples of the AuNPs in THF were drop-cast onto carbon-coated copper mesh grids, purchased from Electron Microscopy Sciences. Figure 2 shows representative images for C6 and C12 particles, along with the associated

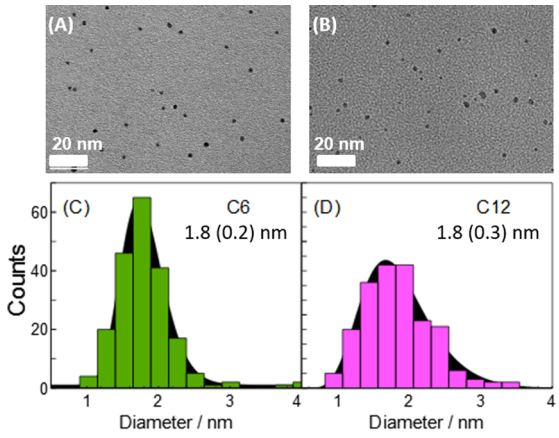

Figure 2. Representative TEM Images and the associated size distribution histograms for C6 (A and C) and C12 (B and D) AuNPs, respectively. Refer to the SI for images and histograms of C4 and C7−C11.

histograms for all images of the two samples. Refer to the SI for full TEM characterization of all samples.

Spectral Fitting Procedure. A detailed account of our spectral fitting procedure can be found elsewhere;[10] however, a brief overview will be given. All CESR spectra were fit to an approximate Dysonian line shape, composed of a linear combination of first derivative Lorentzian dispersion and absorption lineshapes. The commercially available Mathematica 10.0.0 was used to perform the computations, where the Levenberg−Marquardt fitting algorithm with default accuracy and precision goals was employed. Due to irregularities in the baseline, a third order polynomial (neglecting the quadratic term) was incorporated into the approximate Dysonian equation. Initial guesses of 0.33 T and 1×10^{-9} s for the peak position and line width, respectively, were used. All other parameters were given starting guesses of 1.

DOI: 10.1021/jacs.6b09586
J. Am. Chem. Soc. 2016, 138, 15987−15993

Calculations. Ionization potentials of the free alkanethiols, in *n*-hexane and THF, were calculated using a local version of the Amsterdam Density Functional (ADF) program package at the BP86 functional level using a TZP basis set.[15,16]

RESULTS AND DISCUSSION

All AuNPs used in this study were prepared via the standard Brust synthesis.[17] Analysis of TEM images indicated that the average gold core size ranged between 1.7 and 1.8 nm, with standard deviations between 0.2 and 0.3 nm (Table 1).

Table 1. Summary of the Experimental Values Obtained from the Characterization of the Particles and CESR Experiments and Ionization Potentials for the Ligands in Both *n*-Hexane and THF[a]

ligand	size/nm	$IP_{ligand}^{n\text{-hexane}}$/eV	IP_{ligand}^{THF}/eV	$g^{n\text{-hexane}}$	g^{THF}
C4	1.8 (0.3)	7.776	6.659	1.982	1.989
C6	1.8 (0.2)	7.704	6.648	1.975	1.978
C7	1.7 (0.2)	7.673	6.645	1.969	1.969
C8	1.8 (0.2)	7.644	6.643	1.965	1.966
C9	1.7 (0.3)	7.593	6.644	1.963	1.964
C10	1.8 (0.3)	7.543	6.641	1.961	1.963
C11	1.7 (0.2)	7.496	6.637	1.957	1.960
C12	1.8 (0.3)	7.454	6.631	1.955	1.959

[a]Parentheses indicate standard deviation in size. Errors for all g-factors are ±0.001.

Thus, within error, these particles are all the same diameter, and sit near the molecule-to-metal transition for gold.

Response in *n*-Hexane. Continuous-wave (CW) CESR measurements of these particles at X-band frequency (~9.623 GHz) were acquired using *n*-hexane as the solvent. Figure 3A shows the CESR spectra obtained for C6 and C12-protected AuNPs, while the spectra for all of the AuNPs in this solvent are presented in Figure S10. All signals obtained in this study were asymmetric about their center of gravity and broad ($T_2 \approx 10^{-9}$ s; $\Delta B \approx 12$ mT), consistent with the signal anticipated for metallic systems.[18] Thus, though these particles are small enough to lie within the metal-to-molecule transition, the CESR line shape clearly identifies them as metallic. All spectra were fit to an approximate Dysonian function:

$$\frac{d\chi''}{dB} = D\frac{1-(\gamma(B-B_0)T_2)^2}{(1+(\gamma(B-B_0)T_2)^2)^2} - A\frac{2\gamma(B-B_0)T_2}{(1+(\gamma(B-B_0)T_2)^2)^2} \quad (1)$$

where χ'' is the imaginary part of the magnetic susceptibility, B is the magnetic field, D is the dispersion coefficient, A is the absorption coefficient, γ is the electron gyromagnetic ratio, B_0 is the resonance position, and T_2 is the relaxation time. By fitting experimental data with eq 1, B_0 is extracted and converted into the electronic g-factor using the relation, $g = 714.4\ \nu_{mw}/B_0$ (Table 1; ν_{mw} in GHz and B_0 in G). Details of fitting and extraction of the g-factor are given in our previous publication,[10] the results of the fitting for this work are shown in Figure S10, and the extracted g-factors are collected in Table 1. All of the g-factors we obtain are less than those expected for pure gold particles of 1.7−1.8 nm diameter ($g_{bareAuNP}^{1.8nm} = 2.067$),[19] with the g-factor of our particles monotonically decreasing with increasing chain length. The direction of this g-shift away from pure gold is consistent with our prior results, and appears to be a property of the gold−sulfur interface.[10,11]

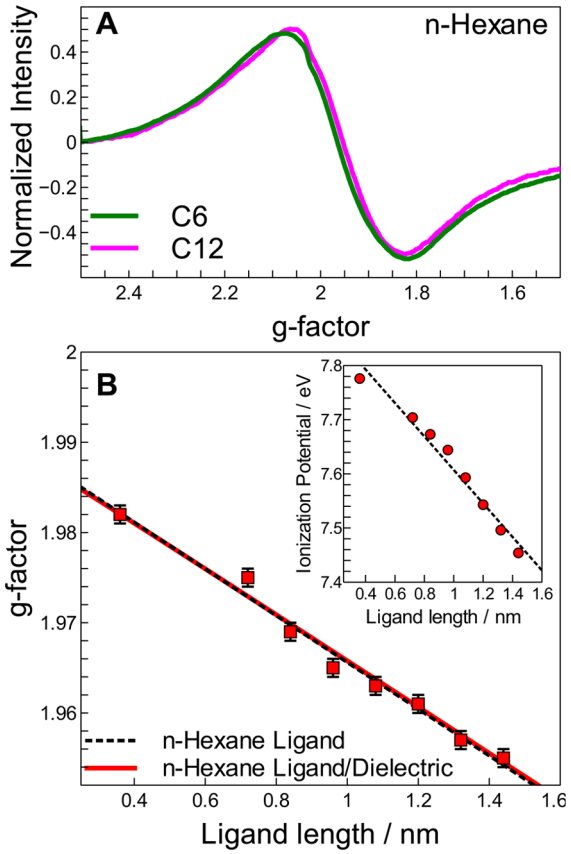

Figure 3. CESR data in *n*-hexane and trends that result from them. (A) Representative X-band CW-CESR spectra collected in *n*-hexane for C6- (green) and C12-protected (magenta) AuNPs plotted as a function of g-factor (measured at 25 K). (B) Plot of the extracted g-factor as a function of the extended ligand length in *n*-hexane. The data is fit to models which take into account the isolated effect of the ligand effect (dashed black line) and a combined ligand/solvent model (red solid line; eq 4). The inset shows the results of DFT-level calculations (in *n*-hexane) for the IP of the free alkanethiol ligand as a function of the ligand's alkyl tail length. The dotted trace is the result of a linear fit to the data using the formula $IP = ml + b$, where l is the ligand length, $b = 7.92$ eV and $m = -0.309$ eV nm^{-1}.

Surprisingly, we find that the g-factor for the AuNPs is responsive to the identity of the hydrocarbon tail group up to 12 carbons in length. A plot of the g-factor versus alkanethiolate chain length (Figure 3B; see Supplementary Section 4 and Figure S12 for calculation of ligand length) can be fit to a line (dashed black line, $R^2 = 0.98$). Remarkably, this means that the effect of changing from C4 to C6 is the same as changing from C10 to C12.

Given that ligand coverage on AuNPs is a function of chain length,[20] it seemed possible that changes in ligand coverage were leading to our observed trend in g-factor. However, analysis of the ligand coverage for our hexanethiol and dodecanethiol protected AuNPs (see SI for details) revealed no difference in ligand coverage for these two nanoparticle systems. This is in agreement with prior work on surface coverage by acid-terminated alkanethiols.[20] Thus, we do not ascribe changes in g-factor to changes in ligand coverage. Instead, we next sought to understand how adding a carbon to the *distal* end of a ligand's aliphatic chain controls the properties of electrons within the metallic core.

DOI: 10.1021/jacs.6b09586
J. Am. Chem. Soc. 2016, 138, 15987−15993

In our prior work on the aromatic thiolates,[11] we worked from the fact that the g-factor is a characterization of spin orbit coupling and proposed that both the electron−core Coulombic attraction (ξ) and the orbital angular momentum ($\hat{L}$) for the electron contribute to the electron's spin−orbit coupling Hamiltonian ($\hat{H}_{SOC}$):[19,21−23]

$$\hat{H}_{SOC} = \xi \hat{L}\cdot\hat{S} \tag{2}$$

where $\hat{S}$ is the electron spin angular momentum operator. As an initial approximation, we do not expect that changes to the length of the alkane chain will significantly impact the electronic band structure of the AuNP's core, because the orbitals involved in the distal end of the alkane chain should not couple into the orbitals found in the gold core. For this reason, we neglect changes to the $\hat{L}$ term. This places the focus on the ξ term. The Coulombic attraction accounted for by this term is related to many other concepts, including the surface potential, charge density, work function, and position of the E_F. In what follows, we choose to use the term surface potential as a stand-in for ξ, though it is important to keep in mind that all of these common metallic properties are interconnected.

Framing the discussion in these terms, our question becomes how does adding a carbon to the distal end of a ligand's aliphatic chain control the *surface potential* of the metallic core? Due to the σ-bonding nature of alkanethiolates on gold, it is expected that a covalent interaction between the thiolate and gold dominates the interfacial interaction.[24,25] Invoking a molecular orbital view of this bond, the relative energy between the *d*-band of the metal and the highest occupied molecular orbital (HOMO) of the ligand will control the amount of charge transferred between the ligand's sulfur and the gold core through the bond and, hence, the surface potential of the metal.[9,26]

To support the above reasoning, we calculated the ionization potential (IP) of the isolated alkanethiols in *n*-hexane. The IP of the bare AuNPs (without ligands) will be a constant, and so the change in IP of the free ligand reflects the expected change in the charge donation across the alkanethiol series. The IPs were calculated in an *n*-hexane continuum using DFT (see SI for details). We find an excellent linear correlation (R^2 = 0.97) between IP and alkane chain length (Table 1, and inset Figure 3B), suggesting that this can be used to explain the linear trend in g-values via charge transfer at the interaface. This conclusion also highlights the critical nature of the Au−S interaction and is satisfying, given the simple line of molecular orbital-based reasoning that we took to arrive at this model.

It is worth emphasizing the fact that our calculations support the observation that the relative effect of increasing from C4 to C6 is the same as the effect of increasing from C10 to C12. Such changes in chain length are not often considered in controlling the electronic structure of organic molecules, metal centers in transition metal complexes, or supramolecular systems. Moreover, the importance of choice of chain length in the synthesis of AuNPs is often also not discussed with respect to the electronic properties of the gold core. However, both our experimental observations and our calculations suggest that changes in chain length are a valid and effective way in which to control the electronic properties of metallic systems, via adjustment of the orbital energy level of the ligand.

In addition to our calculations, the idea that the surface potential of AuNPs might be linearly dependent on alkane chain length is supported by work on self-assembled monolayers (SAMs) of alkanethiolates on a Au(111) surface. These studies have shown that the surface potential is linearly related to the alkyl chain length.[27] Specifically, it was demonstrated that the surface potential of the metal/SAM interface becomes more negative by increasing the length of the chemisorbed alkanethiol, an effect attributed to the formation of an increasing dipole moment associated with the well-ordered monolayer at the surface (Figure 1A), ascribed to increasing the magnitude of the positive end of the dipole moment with chain length, and ultimately leading to a decrease in the work function of the metal.[27,28] However, this interpretation rested upon the assumption of well-ordered monolayers with a changing dielectric constant.[29−31] The fact that we observe similar effects on a highly curved surface, where a high degree of ordering of the alkanes is not necessarily expected,[32,33] suggests that another mechanism (e.g., chemical bonding) is responsible for changes to the electronic properties of the metal. That is, it is the dipole of the interfacial bond (arising from the change in HOMO energy of the thiol) that underpins this change.

Response in THF. That the particle's surface potential is responding to changes in alkane chain length also suggests AuNPs will respond to other subtle chemical changes that are commonly employed for AuNP-based applications, such as altering the dielectric constant of the solvent (Figure 1C). Girault and co-workers have previously shown that the redox potential relative to the absolute vacuum scale ($[E_{ze/(z-1)e}]^{NP}_{AVS}$) for a metallic nanoparticle of radius r, protected with a ligand shell of thickness l and dielectric constant ϵ_l, immersed in a dielectric environment of ϵ_s, is given as

$$e[E^0_{ze/(z-1)e}]^{NP}_{AVS} = \Phi_{bulk} + \frac{(2z-1)e}{8\pi\epsilon_0(r+l)}\left(\frac{\epsilon_l r + \epsilon_s l}{\epsilon_l \epsilon_s r}\right) \tag{3}$$

where Φ_{bulk} is the work function for the bulk metal, ϵ_0 is the relative permittivity of vacuum, e is the elementary unit of charge, and z is the integer charge state—in this study, z will be taken as 1 in order to model the IP of the AuNP.[34] As follows from this equation, unless $\epsilon_l = \epsilon_s$, the thickness of the ligand layer (l) will produce a nonlinear response of the metal core's work function. Because of the connection between work function and surface potential, we should then also observe a nonlinear dependence of the g-factor upon the surfactant thickness. The larger the difference between ϵ_l and ϵ_s is, the stronger the nonlinear effect will be. Note that when $\epsilon_l = \epsilon_s$ eq 3 becomes independent of l, and reduces to a constant. In *n*-hexane, we expect this equality to hold and the dielectric charging to have a negligible influence on the particle. At the same time, the linear response on chain length in *n*-hexane reminds us of the importance of the direct charging from the ligand's IP.

Taking eq 3 and our DFT calculations into consideration, we propose that the g-factor dependence on the alkane chain length should be modeled as

$$g(l) = g' + \alpha\cdot\left\{\frac{(2z-1)e}{8\pi\epsilon_0(r+l)}\left(\frac{\epsilon_l r + \epsilon_s l}{\epsilon_l \epsilon_s r}\right) + \phi\cdot[\mathrm{IP}^{\mathrm{ligand}}_{\mathrm{solvent}}(l)]\right\} \tag{4}$$

In this equation, the terms between the curly brackets reflect the change to the gold core's work function, which is related to the surface potential, $g(l)$ is the observed g-factor of a AuNP protected by a dielectric layer of thickness l, α is a conversion factor between the work function in eV and the g-factor,

DOI: 10.1021/jacs.6b09586
J. Am. Chem. Soc. 2016, 138, 15987−15993

ϕ is a factor that reflects how the IP of the ligands change the work function of the gold core upon binding, and $IP^{ligand}_{solvent}(l)$ accounts for the changes in the IP of the ligand as a function of the ligand length in a given solvent and which can be quantum chemically calculated (Table 1). For this model, we expect both α and ϕ to have a dependence on the size of the particle, via changes to the surface area to volume ratio. The final parameter to consider is g', which is actually composed of several contributions. The easiest of these contributions to define is the contribution that comes from the g-factor expected for a bare AuNP in vacuum (2.067 for 1.8 nm AuNPs).[19] However, g' also accounts for corrections needed due to uncertainties in both the absolute values of the DFT calculations and the nature of the metal/molecule interface. Though g' is used to account for uncertainties in our model, it does not influence the chain length *dependence*.

Eq 4 makes it clear that, as the difference in dielectric constant between the surfactant and solvent increases, the g-factor's dependence on chain length should deviate more strongly from linearity. Acquiring CESR spectra of our nanoparticles in THF (Figure 4A) does indeed yield a set of values for the g-factor

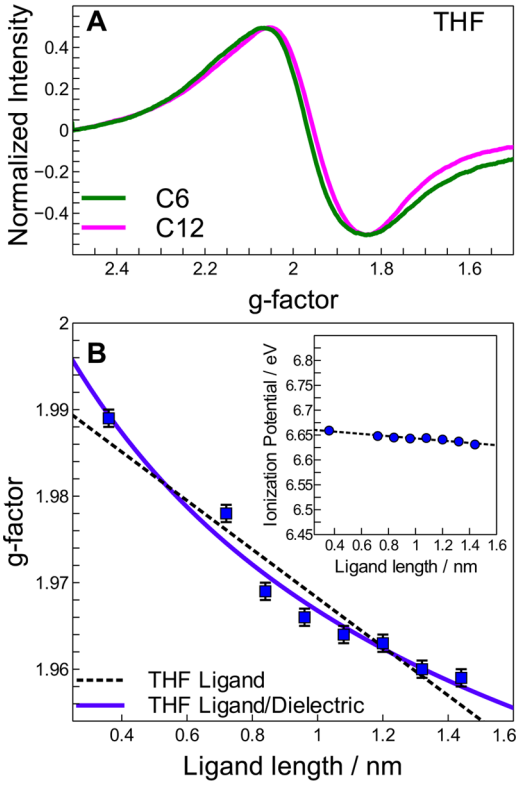

Figure 4. CESR data in THF and trends that result from them. (A) Representative X-band CW-CESR spectra of C6- (green) and C12-protected (magenta) AuNPs in THF (measured at 25 K). (B) The g-factor as a function of ligand length for the AuNPs, collected in THF. Just as in the case of *n*-hexane, the data is fit to a model which takes into account only the ligand effect (dashed black line), and the combined ligand and dielectric effect (blue solid line; eq 4). The inset depicts the DFT-calculated IP of the free ligand in THF, fit to a line IP = $ml + b$, where l is a ligand length, b = 6.67 eV and m = −0.023 eV nm^{-1} (dotted trace). The ordinate of the inset is set to the same scale as in Figure 3B to emphasize the far more mild slope for the THF data.

(Table 1) that are nonlinear with alkane chain length. This is most readily seen in Figure 4B, where fitting the g-factor as a function of chain length with a linear regression produces a poorer linear correlation (R^2 = 0.92) than that found for the particles in *n*-hexane. It is important to recall that, under the interpretation presented by eq 4, the linear response observed in *n*-hexane is a result of the similarity in dielectric constant between *n*-hexane (ϵ = 1.88) and the aliphatic ligands (estimated as 1.9), which essentially removes the dependence on the dielectric constant. Importantly, we can take advantage of the linear correlation in *n*-hexane for interpreting our results in THF since this presents us with an opportunity to iteratively solve for the values of α and ϕ (see SI for details), using the calculated IP values of the ligands to obtain $IP^{ligand}_{solvent}(l)$.

The values we obtain from our iterative fitting are given in Table 2, and the returned fits are shown as solid red (R^2 = 0.98)

Table 2. Extracted Fitting Parameters Using Eq 4 to Fit the g-Factor as a Function of Linear Ligand Length in *n*-Hexane and THF

solvent	α/eV^{-1}	ϕ	g'
n-Hexane	−0.28 ± 0.01	−0.31 ± 0.01	2.111 ± 0.001
THF	−0.28 ± 0.01	−0.31 ± 0.01	2.045 ± 0.006

and blue (R^2 = 0.97) lines in Figures 3 and 4, respectively. Thus, we see that eq 4 produces better fits to the THF compared to a simple linear model, where the dielectric contribution is more pronounced, but similar fits to the linear model for *n*-hexane, where the dielectric contribution is much less important, are obtained. Thus, the simple electrostatic model presented in eq 4 provides a rationale for our results in both *n*-hexane and THF.

It is worth considering the connection between the electrostatic model represented by eq 4 and spin−orbit coupling. Recall that eq 4 is a modification of eq 3, which is an expression related to changes in the work function of a metal in a dielectric medium. Because work function and surface potential are proportional,[35] eq 4 suggests that the g-factor for metallic nanoparticles is closely connected to the surface potential—an idea consistent with previous work on the correlation between surface potential and work function for self-assembled monolayers of alkanethiolates on gold.[27,28] In addition, the good agreement between the trends in our data and the electrostatic model of eq 4 supports our original assumption that dominant effects of changes in the alkyl tail group's length would be related to ξ, which can be approximated as a change in the surface potential. Thus, despite the discrepancies between experiment and theory that lead to the ambiguity in g', and the fact that we ignore changes to orbital angular momentum, we find that the simple ionic model expressed in eq 4 provides good quantitative agreement with both sets of data. This, in turn, allows us to offer general comments on the impact of alkanethiolates over the electronic properties of the AuNPs.

Interpretation of Electrostatic Model. From the perspective of the direct effects of surface chemistry, our work indicates that the primary mechanism behind the relative changes in g-factor is thiolate-to-gold charge transfer, which results in an adjustment of the E_F of the metallic core (Figure 5). The results in *n*-hexane reveal the importance of the IP of the ligands, as it is the linear term in eq 4 which dominates the trend in Figure 3. Following from Koopmans' theorem, the trend from the DFT calculations would indicate that the energy of the ligand's HOMO increases with an increase in chain length. Thus, we

DOI: 10.1021/jacs.6b09586
J. Am. Chem. Soc. 2016, 138, 15987−15993

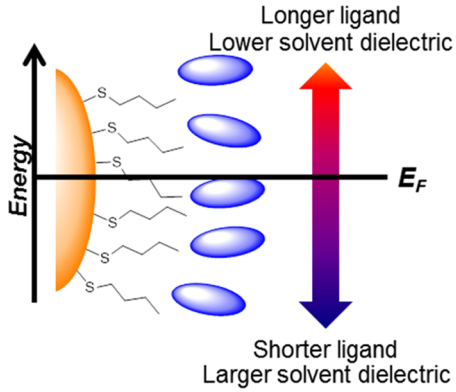

Figure 5. Proposed mechanism for surface potential dependence on g-factor. Increases in the Fermi level (E_F) are accompanied by longer-chain alkanethiolates and lower dielectric solvents, which leads to decreased g-factors. The orange and blue ovals represent the gold surface and solvent, respectively.

hypothesize that we are affecting the g-factor via a direct charge transfer mechanism through increased interfacial mixing between the gold core and the ligand headgroup. This increased mixing should also be correlated with other nanoparticle/ligand properties such as the strength of the chemical bond between gold and sulfur.[36] Changes in bond strength might be expected, as the energy of the HOMO of the thiol changes with chain length. Specifically, increases in the HOMO energy could be expected to lead to stronger binding to the gold surface and a resulting larger degree of charge transfer from the ligand to the metal, in turn leading to the monotonic decrease in g-factor from C4 to C12 that we measure.

As for the dielectric medium, its effect is to modulate the strength of charge transfer, where a solvent with a higher dielectric constant would be capable of decreasing the charge density at the interface. In turn, this decreases the strength of the interfacial bonding interaction and leads to the observed increase in g-factor. In total, this would manifest itself as a decrease in the E_F of the metal, and thus a more positive surface potential (and larger g-factor), as the length of the ligand decreases and the dielectric constant of the solvent increases.

Though the alkyl tail group is not typically thought of as a means to tune electronic properties, our results show it may serve as a chemically inert "handle" to tune the E_F of gold-semiconducting nanoscopic heterodimers. Such systems have garnered much attention in photocatalysis and plasmonic solar cells due to the large extinction cross-section of AuNPs;[4] however, electronic coupling between gold and semiconducting substrates has been shown to be limited.[2,37,38] Size, geometry, and chemical identity of the solid-state materials are commonly exploited as a means for improvement by tuning the relative energies of the valence and conduction band edges in the semiconductor or the E_F of the metal. Our study eludes to an alternative to such manipulations. The existing surface chemistry of the AuNP can be exploited to modulate the relative position of the E_F and improve interfacial electronic coupling of metal–semiconductor junctions, where the paradigm of structure–function manipulation to control the electronic structure of ligands, even beyond the alkyl tail group, would serve as an invaluable tool in the rational design of materials.

Lastly, the solvents examined in this study represent two cases for controlling the electronics properties of the metallic electronics in AuNPs: (1) in *n*-hexane, a solvent similar in dielectric to the ligand, the electronic mixing between the covalently bound alkanethiolate and gold surface dominates the electronic structure of the surface, while (2) in THF, the dielectric of the solvent becomes apparent and provides a secondary influence over the electronic properties of the gold core; in total, the increase in dielectric constant of the environment serves to lower the surface potential of the AuNPs. All of these observations are explained in terms of a simple ionic model (corrected with a linear term that takes into account the electronic structure of the ligands), which reproduces our observed trends.

CONCLUSION

Previous experimental and theoretical work on gold surfaces has suggested that thiolate adsorption leads to charge transfer across the metal/ligand interface of AuNPs.[39,40] We have now directly probed this charge transfer for alkanethiolates on gold, without accessing electronically excited or ionized states. Additionally, though the effects of chain length upon electronic properties of metals have been hinted at, our work isolates the importance of direct effects of the interfacial chemical bond (i.e., charge transfer) in tuning the electronic properties of the metallic core in AuNPs. Our CESR measurements indicate that as we increase the chain length of the appended alkanethiolate, we increase the charge density of the metallic core, and thus, raise the Fermi level. Furthermore, by changing the properties of the dielectric environment (i.e., the solvent), the electronic properties of the metallic core can also be modified, such that a less polar solvent leads to an increase in the Fermi level. To the extent that it is desirable to control electron/hole conductance at molecule/metal junctions, extend the lifetime of excited spin states through suppression of spin–orbit coupling for optomagnetic data storage in spintronics, or predict the relative redox potential of nanoplasmonic materials for photocatalysis, our findings provide new insight into how this can be accomplished through surface chemical modification of the ligand sphere.

ASSOCIATED CONTENT

Supporting Information

The Supporting Information is available free of charge on the ACS Publications website at DOI: 10.1021/jacs.6b09586.

TEM (images and log-normal) + CESR (spectra, fits, and residuals), the experimental section, the ligand length calculation, and determination of relative surface coverage of ligands (PDF)

AUTHOR INFORMATION

Corresponding Author

*bul14@psu.edu

Notes

The authors declare no competing financial interest.

ACKNOWLEDGMENTS

The authors thank the Pennsylvania State University for funding. L.J. acknowledges support from the NSF award CHE-1362825. B.J.L acknowledges funding from NSF award CHE-1609572.

REFERENCES

(1) Leary, E.; Rosa, A. L.; González, T.; Rubio-Bollinger, G.; Agraït, N.; Martin, N. *Chem. Soc. Rev.* **2015**, *44*, 920–942.
(2) Wu, K.; McBride, J.; Lian, T. *Science* **2015**, *349*, 632–635.

DOI: 10.1021/jacs.6b09586
J. Am. Chem. Soc. 2016, 138, 15987–15993

(3) Stewart, M.; Anderton, C.; Thompson, L.; Maria, J.; Gray, S.; Rogers, J.; Nuzzo, R. *Chem. Rev.* **2008**, *108*, 494−521.
(4) Jain, P. K.; Huang, X.; El-Sayed, I. H.; El-Sayed, M. A. *Plasmonics* **2007**, *2*, 2:107−2:118.
(5) Peng, S.; McMahon, J. M.; Schatz, G. C.; Gray, S. K.; Sun, Y. *Proc. Natl. Acad. Sci. U. S. A.* **2010**, *107*, 14530−14534.
(6) Kelly, K.; Coronado, E.; Zhao, L.; Schatz, G. *J. Phys. Chem. B* **2003**, *107*, 668−677.
(7) Trudel, S. *Gold Bull.* **2011**, *4*, 4:3−4:13.
(8) Aruda, K. O.; Tagliazucchi, M.; Sweeney, C. M.; Hannah, D. C.; Schatz, G. C.; Weiss, E. A. *Proc. Natl. Acad. Sci. U. S. A.* **2012**, *110*, 4212−4217.
(9) Goldmann, C.; Lazzari, R.; Paquez, X.; Boissière, C.; Ribot, F.; Sanchez, C.; Chanéac, C.; Portehault, D. *ACS Nano* **2015**, *9*, 7572−7582.
(10) Cirri, A.; Silakov, A.; Lear, B. J. *Angew. Chem., Int. Ed.* **2015**, *54*, 11750−11753.
(11) Cirri, A.; Silakov, A.; Jensen, L.; Lear, B. J. *Phys. Chem. Chem. Phys.* **2016**, *18*, 25443−25451.
(12) Crawford, S. E.; Andolina, C. M.; Smith, A. M.; Marbella, L. E.; Johnston, K. A.; Straney, P. J.; Hartmann, M. J.; Millstone, J. E. *J. Am. Chem. Soc.* **2015**, *137*, 14423−14429.
(13) Hostetler, M. J.; Wingate, J. E.; Zhong, C.-J.; Harris, J. E.; Vachet, R. W.; Clark, M. R.; Londono, J. D.; Green, S. J.; Stokes, J. J.; Wignall, G. D.; Glish, G. L.; Porter, M. D.; Evans, N. D.; Murray, R. W. *Langmuir* **1998**, *14*, 17−30.
(14) Hicks, J. F.; Templeton, A. C.; Chen, S.; Sheran, K. M.; Jasti, R.; Murray, R. W. *Anal. Chem.* **1999**, *71*, 3703−3711.
(15) Guerra, C. F.; Snijders, J. G.; te Velde, G.; Baerends, E. J. *Theor. Chem. Acc.* **1998**, *99*, 391−403.
(16) te Velde, G.; Bickelhaupt, F. M.; Baerends, E. J.; Guerra, C. F.; van Gisbergen, S. J. A.; Snijders, J. G.; Ziegler, T. *J. Comput. Chem.* **2001**, *22*, 931−967.
(17) Brust, M.; Walker, M.; Bethell, D.; Schiffrin, D. J.; Whyman, R. *J. Chem. Soc., Chem. Commun.* **1994**, *0*, 801−802.
(18) Edmonds, R. N.; Harrison, M. R.; Edwards, P. P. *Annu. Rep. Prog. Chem., Sect. C: Phys. Chem.* **1985**, *82*, 265−308.
(19) Buttet, J.; Car, R.; Myles, C. W. *Phys. Rev. B: Condens. Matter Mater. Phys.* **1982**, *26*, 2414−2431.
(20) Hinterwirth, H.; Kappel, S.; Waitz, T.; Prohaska, T.; Lindner, W.; Lämmerhofer, M. *ACS Nano* **2013**, *7*, 1129−1136.
(21) Sone, J. *J. Phys. Soc. Jpn.* **1977**, *42*, 1457−1462.
(22) Rotenberg, E.; Chung, J.; Kevan, S. *Phys. Rev. Lett.* **1999**, *82*, 4066−4069.
(23) Petersen, L.; Hedegård, P. *Surf. Sci.* **2000**, *459*, 49−56.
(24) Bourg, M.; Badia, A.; Lennox, R. *J. Phys. Chem. B* **2000**, *104*, 6562−6567.
(25) Heimel, G.; Romaner, L.; Zojer, E.; Bredas, J.-L. *Acc. Chem. Res.* **2008**, *41*, 721−729.
(26) Hoffmann, R. *Solids and Surfaces: A Chemista's View of Bonding in Extended Structures*; Wiley-VCH, 1989.
(27) Evans, S. D.; Ulman, A. *Chem. Phys. Lett.* **1990**, *170*, 462−466.
(28) Lee, H.; Jamison, A.; Lee, T. *Acc. Chem. Res.* **2015**, *48*, 3007−3015.
(29) Terrill, R.; Postlethwaite, T.; Chen, C.; Poon, C.; Terzis, A.; Chen, A.; Hutchinson, J.; Clark, M.; Wignall, G.; Londono, J.; Superfine, R.; Flavo, M.; Johnson, C. S.; Samulski, E.; Murray, R. *J. Am. Chem. Soc.* **1995**, *117*, 12537−12548.
(30) Hostetler, M.; Stokes, J.; Murray, R. *Langmuir* **1996**, *12*, 3604−3612.
(31) Badia, A.; Cuccia, L.; Demers, L.; Morin, F.; Lennox, R. *J. Am. Chem. Soc.* **1997**, *119*, 2682−2692.
(32) Hostetler, M.; Stokes, J.; Murray, R. *Langmuir* **1996**, *12*, 3604−3612.
(33) Weeraman, C.; Yatawara, A.; Bordenyuk, A.; Benderskii, A. *J. Am. Chem. Soc.* **2006**, *128*, 14244−14245.
(34) Scanlon, M. D.; Peljo, P.; Mendez, M. A.; Smirnov, E.; Girault, H. H. *Chem. Sci.* **2015**, *6*, 2705−2720.
(35) Su, B.; Girault, H. *J. Phys. Chem. B* **2005**, *109*, 11427−11431.
(36) Albright, T.; Burdett, J.; Whangbo, M. *Orbital Interactions in Chemistry*; John Wiley and Sons, 1985.
(37) Wu, K.; Rodrìguez-Còrdoba, W.; Yang, Y.; Lian, T. *Nano Lett.* **2013**, *13*, 5255−5263.
(38) Zhang, Y.; Yam, C.; Schatz, G. *J. Phys. Chem. Lett.* **2016**, *7*, 1852−1858.
(39) Häkkinen, H. *Nat. Chem.* **2012**, *4*, 443−455.
(40) Büttner, M.; Kröger, H.; Gerhards, I.; Mathys, D.; Oelhafen, P. *Thin Solid Films* **2006**, *495*, 180−185.

DOI: 10.1021/jacs.6b09586
J. Am. Chem. Soc. 2016, 138, 15987−15993